Environmental Science & Technology

pubs.acs.org/est

Article

Mercury Uptake, Accumulation, and Translocation in Roots of Subtropical Forest: Implications of Global Mercury Budget

Wei Yuan, Xun Wang,* Che-Jen Lin, Fei Wu, Kang Luo, Hui Zhang, Zhiyun Lu, and Xinbin Feng*

Cite This: *Environ. Sci. Technol.* 2022, 56, 14154−14165

Read Online

ACCESS | Metrics & More | Article Recommendations | Supporting Information

ABSTRACT: Plant roots are responsible for transporting large quantities of nutrients in forest ecosystems and yet are frequently overlooked in global assessments of Hg cycling budgets. In this study, we systematically determined the distribution of total Hg mass and its stable isotopic signatures in a subtropical evergreen forest to elucidate sources of Hg in plant root tissues and the associated translocation mechanisms. Hg stored in roots and its isotopic signatures show significant correlations to those found in surrounding soil at various soil depths. The odd mass-independent fractionation (MIF) of root Hg at a shallow soil depth displays a −0.10‰ to −0.50‰ negative transition compared to the values in aboveground woody biomass. The evidence suggests that root Hg is predominantly derived from surrounding soil, rather than translocation of atmospheric uptake via aboveground tissues. The cortex has a more negative mass-dependent fractionation (MDF) of −0.10‰ to −1.20‰ compared to the soil samples, indicating a preferential uptake of lighter isotopes by roots. The similar MDF and odd-MIF signals found in root components imply limited Hg transport in roots. This work highlights that Hg stored in plant roots is not a significant sink of atmospheric Hg. The heterogeneous distribution of Hg mass in roots of various sizes represents a significant uncertainty of current estimates of Hg pool size in forest ecosystems.

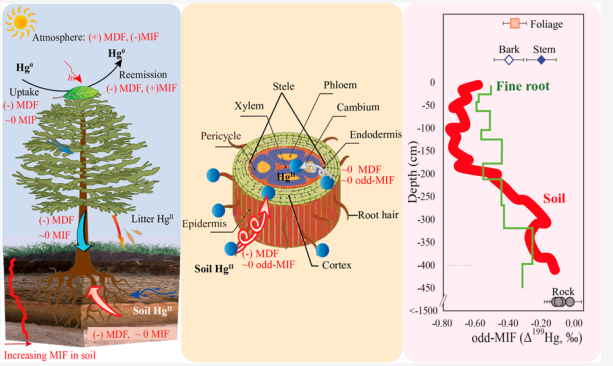

KEYWORDS: *mercury, isotopes, plant roots, root mercury sources, translocation*

1. INTRODUCTION

Mercury (Hg) is a persistent pollutant that leads to health and ecological concerns globally. To protect human health and the environment from global Hg pollution, the Minamata Convention on Mercury, a legally binding international treaty, entered into force in August 2017. However, knowledge gaps of Hg cycling in forest ecosystems limit assessment regarding the effectiveness of anthropogenic emission reduction on human and wildlife Hg exposure.[1,2] Globally, forest ecosystems represent a large atmospheric sink (with 2100−3200 Mg yr^{-1}) of total mercury (Hg^0), which can remove 40%−65% of the total burden in the atmosphere (~5000 Mg) annually[3,4], and which is equivalent to the global anthropogenic Hg emission (1900−2200 Mg yr^{-1}).[1,2] The global sink of atmospheric Hg^0 by vegetation foliage is in the range of 1000−1500 Mg yr^{-1}.[5−8] The global Hg pool size in aboveground woody tissues (branch, bole wood, and bark) is estimated to be 1200−1930 Mg,[3] with an assimilation flux at 177 ± 61 Mg yr^{-1}.[8] However, the storage pool and source of underground roots is less understood. Given the unknown contribution of Hg sources in roots leading to large uncertainties in assessing the atmospheric Hg^0 sink in forests, we aim to better understand how Hg accumulate in roots and the source of Hg in forest ecosystems.

The living biomass in global roots is up to 142 ± 32 Pg in dry mass, accounting for ~22% of the total biomass of aboveground and underground, suggesting the importance of roots in nutrient cycling.[9,10] The root zone is heterogeneous in structure and functions and largely depends on the tree species and environmental conditions. Basically, the fine roots (i.e., root diameter less than 2 mm) and their mycorrhizae obtain nutrients and water, while coarse roots support the root network and deliver nutrients and water to shoots or aboveground tissues and the plant structure.[11] Fine roots usually have a shorter lifespan, greater respiration rate, and higher frequency of mycorrhizal fungi infection, which are all closely related to root function in regard to water and nutrient uptake.[11] Earlier studies showed much higher Hg concentration in fine roots than in coarse roots and suggested that the root morphological traits and functions play important roles in controlling Hg accumulation and uptake in roots.[12,13]

Received: June 13, 2022
Revised: August 23, 2022
Accepted: September 8, 2022
Published: September 23, 2022

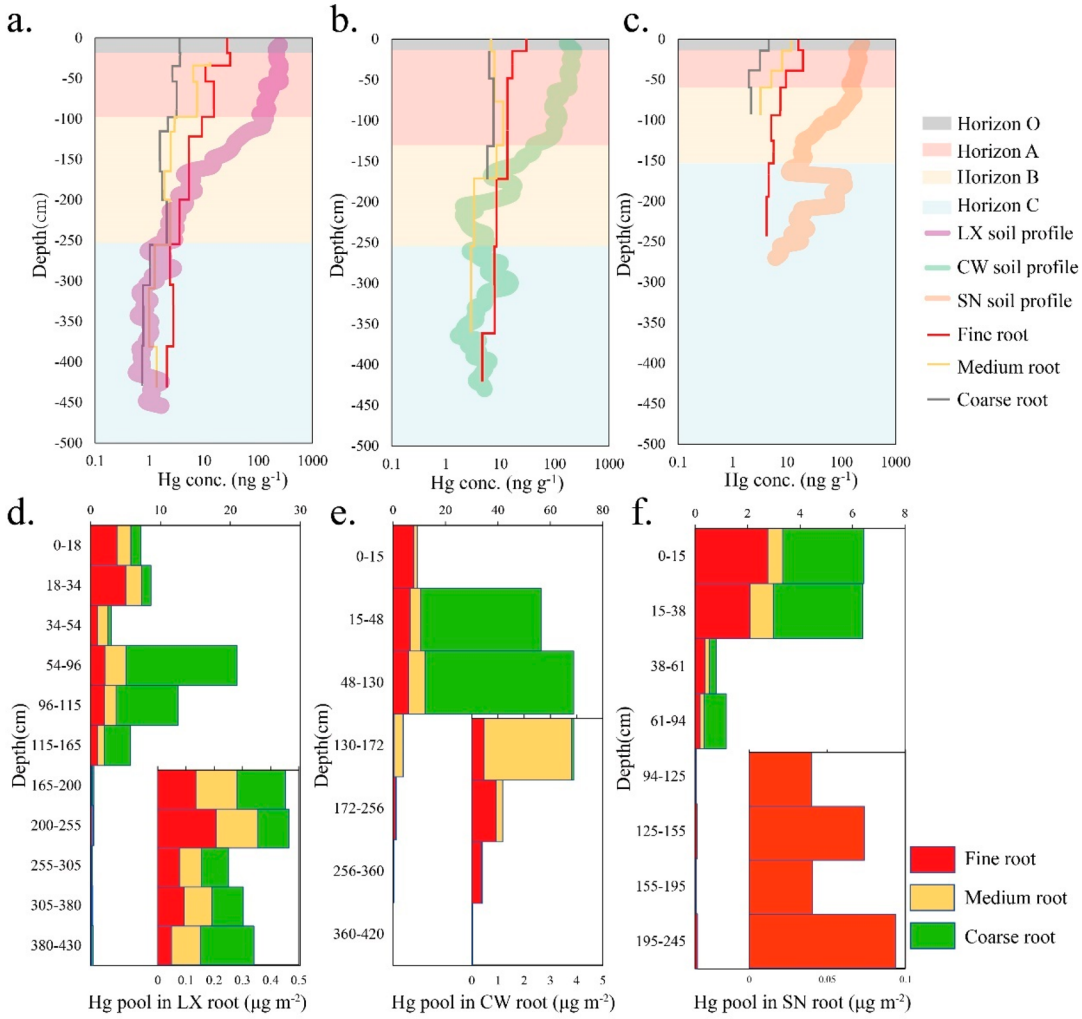

Figure 1. Vertical profiles of investigated variables with soil depth: (a−c) total Hg concentration in roots and (d−f) Hg pool in roots. The embedded figures in d−f use the lower horizontal axis.

However, data describing the role of roots in controlling Hg budget and cycling have been largely lacking due to the difficulty in sampling and in situ measurements.

Currently, the global Hg mass stored in roots is estimated to be 2100−3200 Mg.[3] The large uncertainties are due to data scarcity of root Hg concentrations, specifically those in deep roots. Although data for shallow roots were reported in earlier studies,[3,8] the distribution of the Hg concentration in roots of various sizes has been largely unknown.[12,14] There are also mixed assessments regarding Hg sources in roots. The Hg concentration in global roots is in the range of 2−70 ng g^{-1} in the remote forest, up to an order of magnitude lower than the Hg concentration in surrounding soils.[3,4] Several studies suggested that Hg in roots is mainly from soils, and up to 70% of root Hg uptake can be translocated into foliage and then emitted to the atmosphere during the growing season.[15−20] In contrast, other studies reported that a fraction of Hg in roots could be derived from the translocation of aboveground tissues after uptake of atmospheric Hg^0.[21−24] A recent study estimated that the Hg mass translocated to roots from foliar uptake of atmospheric Hg^0 is ∼300 Mg yr^{-1}.[4]

Signatures of stable Hg isotopes, such as mass-dependent fractionation (MDF, reported as δ^{202}Hg) and mass-independent fractionation (MIF, reported as Δ^{199}Hg and Δ^{201}Hg for odd-MIF and Δ^{200}Hg for even-MIF), offer effective insights to understand Hg sources in roots. Hg^0 in air and foliage in remote forests usually displays predominantly negative odd-MIF and slightly negative even-MIF signatures (around −0.05‰).[3,5,6,14,25−27] However, there is an ∼3% negative fractionation of δ^{202}Hg in foliage compared to air due to MDF that occurs during foliage uptake of atmospheric Hg^0.[5,6] Forest floor soil shows slightly negative odd-MIF, consistent even-MIF signatures as the foliage,[26−29] and various MDF signatures due to the complexity of Hg biogeochemical processes in soils.[26−28] Hg^{II} in precipitation exhibits negative MDF and positive odd-MIF and even-MIF signals,[5,30−32] while Hg^{II} from bedrock shows negative MDF and negligible odd-MIF and even-MIF signals.[33−36]

Given the limited Hg mass translocated from foliage to other aboveground tissues,[14,37] we hypothesize that Hg in plant roots is predominantly derived from forest soil, rather than from foliage. In this study, the concentration of Hg, its vertical distribution, and the isotopic compositions of root Hg were investigated in a subtropical forest to understand the uptake, accumulation, and translocation of Hg in roots. The pathway of root Hg uptake inferred the correlations between Hg and indicative trace elements in roots and soils. Considering that broad-leaved evergreen forest has the largest distribution area

https://doi.org/10.1021/acs.est.2c04217
Environ. Sci. Technol. 2022, 56, 14154−14165

of global tree cover (~29%),[38] the implications on the global underground Hg mass budget in forests were discussed.

2. METHODOLOGY

2.1. Site Description. The studied site is located at the Ailaoshan Station for Subtropical Forest Ecosystem Research Studies (ASSFERS, 24°32′ N, 101°01′ E, 2476 m elevation), Yunnan Province, Southwest China, which has been described in detail elsewhere.[6,39−41] Briefly, ASSFERS has a subtropical monsoon climate, with an annual mean temperature of 11.3 °C and a precipitation depth of ~1800 mm yr^{-1}.[39,42] The dominant tree species are *Lichocarpus xylocarpus* (LX), *Scima noronhae* (SN), *Castanopsisi wattii* (CW), and *Manglietia insignis* with an average canopy height of ~23 m.[39,43] The forest surface soil is mainly alfisols with a pH of 3.5−4.0, containing ~70% sand, 20%−25% silt, and 5%−10% clay.[28,44] In addition, the bedrock is dominated by slate.

2.2. Sample Collections. We set three 1 m × 1 m quadrats for the sampling at ASSFERS. Each quadrat was set on relatively flat forest floor and 0.5 m away from the trunk of the three dominant tree species (LX, SN, and CW) with the average diameter at breast height (DHB, 1−1.5 m) at the ASSFERS. We then dug the quadrat to the depth of the weathered bedrock and sampled the vertical soil profile for SN (270 cm deep), CW (430 cm deep), and LX (450 cm deep), depending on the nature of the sites. For the geogenic Hg samples, we drilled the hole to the depth of 15−20 m of the soil profiles nearby to collect the unweathered slate which was absolutely without any Hg leaching from the upper soils. Based on the soil color and texture, the soil profiles can be divided into humified organic soil (horizon O, gray black), upper eluvial soil (horizon A-upper, gray yellow), lower eluvial soil (horizon A-lower, golden yellow), upper illuvial soil (horizon B-upper, yellow), lower illuvial soil (horizon B-lower, light yellow), highly weathered slate (horizon C-upper), partially weathered slate (horizon C-middle), and slightly weathered slate (horizon C-lower), as shown in Figure 1. The detailed description of the soil profile is provided in the SI, Section 1.

For the root sample collection, we harvested all roots in 1 m × 1 m quadrats with a 40−50 cm depth interval depending on the soil horizon, and then divided the roots into three class orders: fine (diameter < 2 mm), medium (2 mm < diameter < 10 mm), and coarse (diameter > 10 mm). The total root dry mass is shown in Table S1. We found no roots by visual inspection below 420 cm for CW, 245 cm for SN, and 430 cm for LX. We sampled the soil profile with an interval of 5 cm with a 100 cm^3 volume and a 50 mm height cutting ring at each quadrat. Samples of aboveground woody biomass and bark were also collected at DHB of the same tree to assess the potential Hg translocation pathway between aboveground and underground biomass.

After sample collection, we carefully washed the root samples to remove the soil using double distilled water. To measure Hg translocation between the root cortex and stele, we used a stainless-steel blade to dissect the parts of the collected roots into root cortex and stele. Earlier studies showed that oven drying below 50 °C did not lead to distinct Hg loss (<1%) from soil and woody biomass.[14] Hence, all soil and root samples were dried at 45 °C in an oven for 3−4 days until there was no observable moisture weight loss. Finally, all soil samples were ground with an agate mortar and sieved with a 200-mesh (74 μm) nylon screen. Vegetation samples were ground to a fine powder by a precleaned grinder and sieved with a 120-mesh (125 μm) nylon screen.

2.3. Measurements. Mercury concentrations in vegetation and soil samples were measured using a DMA-80 Hg analyzer, following the protocol described in our earlier studies.[14,26,45] The method recovery was determined to be 100.3 ± 3.1% (mean ± SD, n = 37, 95.2%−105.9%) for soil samples using a certified soil reference material GBW07405 (GSS-5, Hg concentration: 290 ± 30 ng g^{-1}) and 100.2 ± 2.6% (mean ± SD, n = 38, 93.3%−105.4%) for vegetation samples using a certified plant reference material GBW10020 (GSB-11, Hg concentration: 150 ± 20 ng g^{-1}). The replicated sample was measured in every nine samples with a bias less than 5%.

The preconcentrations and measurements of Hg isotopes in soil and vegetation samples have been described earlier.[28,35] All samples were processed by double-stage heating pyrolysis in a tube muffle furnace[46] with 5 mL of oxidizing trapping solution of a 40% mixture of concentrated nitric and hydrochloric acid ("reverse aqua regia", HNO_3:HCl = 2:1, v/v). The pure oxygen gas flows were set as 25 mL min^{-1} for soil combustion[47] and increased to 50 mL min^{-1} for root and stem samples for complete combustion. In addition, the temperature programming of the first combustion furnace was carried out for soil samples with a temperature increase of 10 °C min^{-1} for temperature ranges of 25−250 and 650−950 °C and 2.5 °C min^{-1} for 250−650 °C.[28] For plant samples, a temperature increments of 10 °C min^{-1} for temperature ranges of 25−150 and 650−950 °C, 1 °C min^{-1} for 150−250 °C, and 2.5 °C min^{-1} for 250−650 °C were programmed. The Hg concentration enriched in the trapping solution was measured by cold vapor atomic fluorescence spectrometry using U.S. EPA Method 1631.[48] The preconcentration recovery was determined to be 91%−103% by using a soil-certified reference material (GSS-4 with Hg content 590 ± 50 ng g^{-1}) and using a certified vegetative biomass reference (BCR-482 with Hg content 480 ± 20 ng g^{-1}) and 90%−105% for soil and root samples.

The Hg isotope compositions were measured by a multicollector inductively coupled plasma mass spectrometer (MC-ICPMS, Neptune II, Thermo Scientific, USA). The enriched trapping solution was diluted to 0.5 ng mL^{-1} (10% acidity) and was then reduced by 3% $SnCl_2$ to Hg^0 in a cold vapor phase separator, which is consistent with our previous laboratory system.[26,49] A Tl standard (NIST SRM 997) was coupled into the plasma as aerosol particulate through a CETAC Ardius II desolvating nebulizer system. From Bergquist and Blum,[50] the Hg MDF is reported as

$$\delta^{202}\mathrm{Hg}(‰) = [(^{202}\mathrm{Hg}/^{198}\mathrm{Hg})_{\mathrm{sample}}/(^{202}\mathrm{Hg}/^{198}\mathrm{Hg})_{\mathrm{ref}} - 1] \times 1000 \quad (1)$$

MIF is calculated as

$$\Delta^{xxx}\mathrm{Hg}(‰) = \delta^{xxx}\mathrm{Hg} - \delta^{202}\mathrm{Hg} \times \beta_{xxx} \quad (2)$$

where β_{xxx} is 0.252 for ^{199}Hg, 0.502 for ^{200}Hg, and 0.752 for ^{201}Hg, respectively. $(^{202}\mathrm{Hg}/^{198}\mathrm{Hg})_{\mathrm{ref}}$ represents the isotopic ratio in the standard sample (i.e., NIST-3133). The NIST-8610 standard solution was measured every 10−15 samples as a secondary standard with results of δ^{202}Hg = −0.50 ± 0.05‰, Δ^{199}Hg = −0.02 ± 0.04‰, Δ^{200}Hg = 0.02 ± 0.08‰, and Δ^{201}Hg = −0.03 ± 0.05‰ (±2σ, n = 28) and results for BCR-482 (δ^{202}Hg = −1.49 ± 0.03‰, Δ^{199}Hg = −0.62 ± 0.09‰,

https://doi.org/10.1021/acs.est.2c04217
Environ. Sci. Technol. 2022, 56, 14154−14165

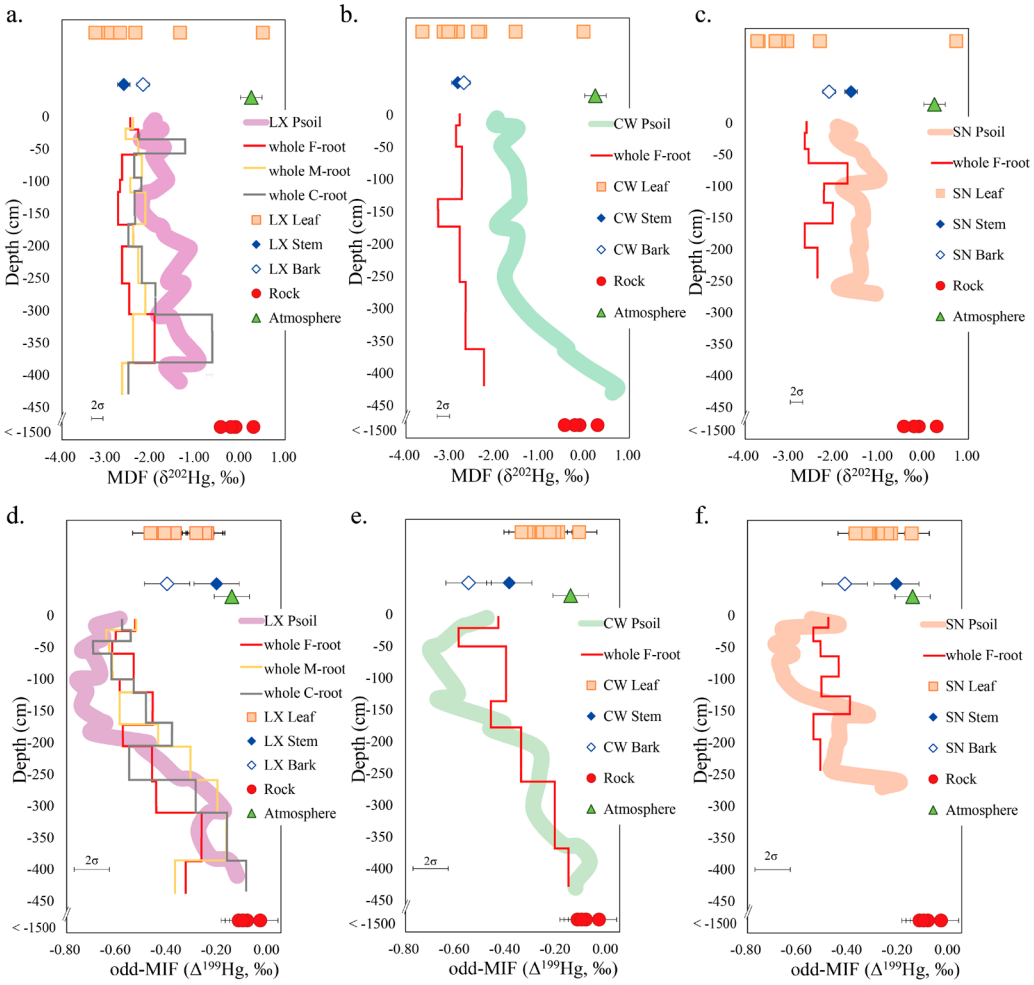

Figure 2. Vertical profiles of the investigated mercury isotopic signatures [(a−c) Δ^{199}Hg and (d−f) δ^{202}Hg] of Hg^{II} in roots (fine, red lines; medium, yellow lines; coarse, gray lines) in soil profiles (LX, purple filled strip; CW, light green filled strip; SN, orange filled strip), in bedrock (red filled circles), in foliage[6] (orange filled square), in bark (blue hollow diamonds), and in stem (blue filled diamonds) and Hg^0 in atmosphere[6,41,49] (green filled triangles). The error bars represent ±2 standard deviation.

Δ^{200}Hg = 0.05 ± 0.08‰, and Δ^{201}Hg = −0.58 ± 0.12‰, ± 2σ, n = 6) and GSS-4 (δ^{202}Hg = −1.60 ± 0.05‰, Δ^{199}Hg = −0.46 ± 0.03‰, Δ^{200}Hg = 0.00 ± 0.06‰, and Δ^{201}Hg = −0.42 ± 0.06‰, ± 2σ, n = 6). These signatures are consistent with the reported values.[26,28,51] The data validate preconcentration by using double-stage offline combustion trapping.

Concentrations of aluminum (Al), iron (Fe), and calcium (Ca) were measured by inductively coupled plasma optical emission spectroscopy (ICP-OES). Concentrations of rubidium (Rb), strontium (Sr), and barium (Ba) were analyzed by inductively coupled plasma mass spectrometry (ICP-MS, Agilent-7900) using U.S. EPA Method 6020B. Briefly, 0.1 g of of each soil and vegetation sample was digested in a closed Teflon vessel by the digestion acid (HNO_3:HF = 5:1, v:v). Each digested solution was then transferred and diluted with ultrapure water to a 50 mL Teflon (PTFE) bottle. The soil standard (GSS-5) and plant standard samples (GSB-11) were digested and measured for QA/QC (quality assurance and quality control).[45] The mean recovery of GSS-5 was 103.8 ± 1.5% for Al, 103.1 ± 1.3% for Fe, 110.5 ± 9.2% for Ca, 102.6 ± 1.1% for Rb, 100.8 ± 1.4% for Sr, and 98.6 ± 0.6% for Ba. The mean recovery of GSB-11 was 104.2 ± 8.3% for Al, 93.7 ± 1.4% for Fe, 105.8 ± 8.5% for Ca, 96.6 ± 6.3% for Rb, 90.1 ± 1.1% for Sr, and 95.7 ± 1.0% for Ba. The signals of the system and reagent blanks were less than 1% of the sample signal for all measurements.

The Hg concentration enrichment factor (EF) for the root tissue and soil is calculated as

$$\mathrm{EF\ Hg_{tissue/soil}} = \mathrm{Conc.\ Hg_{tissue}}/\mathrm{Conc.\ Hg_{soil}} \quad (3)$$

where Conc. Hg_{tissue} and Conc. Hg_{soil} represent the Hg concentrations in root tissue (stele and cortex) and soil, respectively. The Hg MDF isotopic enrichment factor (ε^{202}Hg) of root tissue and soil is estimated as

$$\varepsilon^{202}\mathrm{Hg_{tissue/soil}} = \delta^{202}\mathrm{Hg_{tissue}} - \delta^{202}\mathrm{Hg_{root}} \quad (4)$$

where $\delta^{202}Hg_{tissue}$ and $\delta^{202}Hg_{root}$ represent the Hg MDF isotopic signatures in root tissue and soil, respectively.

3. RESULTS

3.1. Hg Concentration Distribution in Soils and Roots. The soil Hg concentrations of three soil profiles displayed consistent decreasing trends from the O to B horizons (0−250 cm for LX profile and CW profile and 0−150 cm for SN profile, Figure 1a−c). The soil Hg concentration decreased from 200 to 250 ng g^{-1} in the O horizon to 1−10 ng g^{-1} in the B horizon (Table S1). In the C horizon, Hg

https://doi.org/10.1021/acs.est.2c04217
Environ. Sci. Technol. 2022, 56, 14154−14165

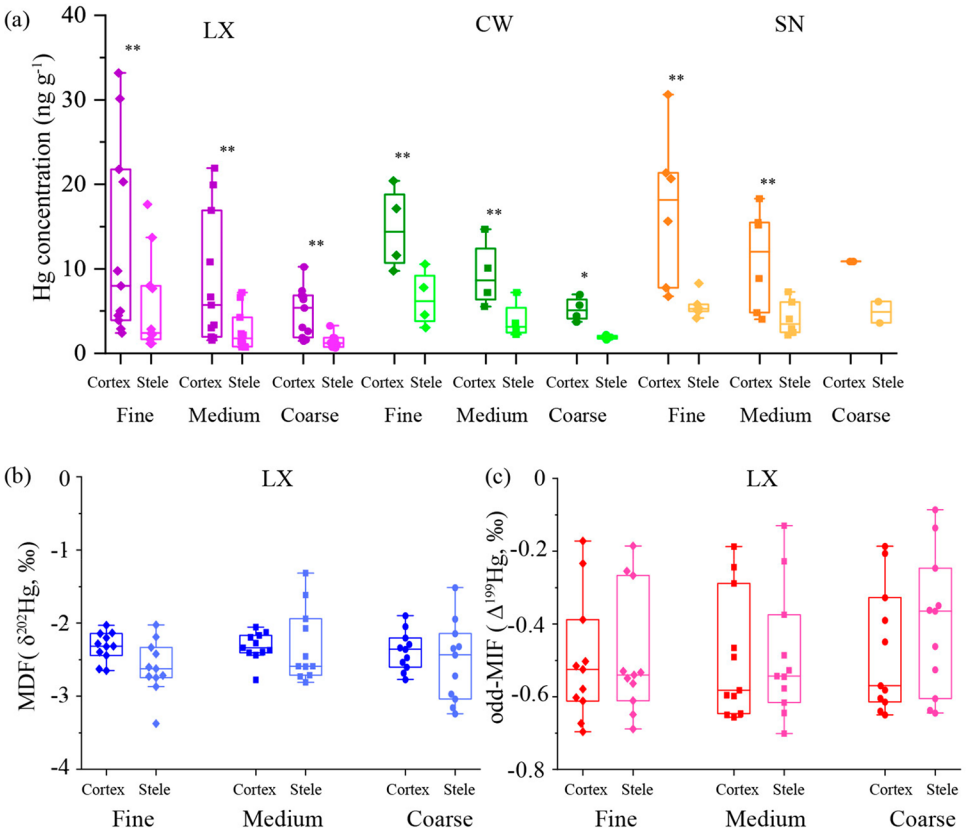

Figure 3. Box charts of (a) Hg concentrations, (b) Hg root MDF signatures, and (c) Hg root Hg odd-MIF signatures in cortex and stele among fine, medium, and coarse roots. ** represents $p < 0.01$ by paired t test, and * represents $p < 0.05$ by paired t test.

concentration of the LX (0.6−2.8 ng g^{-1}, 1.1 ± 0.4 ng g^{-1}) and CW (1.7−15.5 ng g^{-1}, 5.2 ± 3.2 ng g^{-1}) profiles were close to the concentration in bedrock (4.2 ± 1.4 ng g^{-1}) (Table S2). However, we observed elevated Hg concentrations (68.5−106.1 ng g^{-1}) during the depth of 165−205 cm of the SN profiles, which were 5−10 times higher than that in other depths of the C horizon.

The Hg concentrations in roots were nearly 1 order of magnitude lower than concentrations in O−B horizons (Figure 1a−c). The Hg concentrations in roots followed a descending order of fine roots (2.2−29.2 ng g^{-1}, median = 8.6 ng g^{-1}) > medium roots (0.9−13.2 ng g^{-1}, median = 5.2 ng g^{-1}) > coarse roots (0.7−7.4 ng g^{-1}, median = 2.5 ng g^{-1}) ($p < 0.05$ by paired t test). Across the soil profile at three quadrats, the Hg concentration throughout the entire root system demonstrated this decreasing trend. Furthermore, the concentration in fine roots decreased from 17.2 to 28.8 ng g^{-1} at the surfaces of soils to 2.2−4.8 ng g^{-1} at the 420−430 cm soil depth. We found the medium and coarse roots distributed along the 0−430 cm depth at the LX site, 50−170 cm at the CW site, and 0−100 cm at the SN site (Table S3). For vertical Hg distribution, the Hg concentration of medium roots decreased from 7.2 to 12.1 to 1.3−3.5 ng g^{-1} and for coarse roots decreased from 3.7 to 6.5 to 0.7−6.0 ng g^{-1}. Multiplying the Hg concentration and root dry biomass, we estimated the root Hg pool size shown in Figure 1d−f. The total root Hg pool sizes were 59.9 $\mu g\ m^{-2}$ for LX, 140.3 $\mu g\ m^{-2}$ for CW, and 15.1 $\mu g\ m^{-2}$ for SN. The coarse roots accounted for 50.1%−73.2% of the total root Hg pool size, followed by fine roots (15.9%−37.7%). The root Hg pool size mainly clustered at the surface to the 100−150 cm depth of the soil, accounting for 66%−96% of the root total Hg. It is noted that the root Hg storage estimated in this work may not represent the average root Hg pool size at the ASSFERS due to the sampling methodology and limited sampling sites. The reported distribution patterns and relative proportions of fine, medium, and coarse roots illustrate the relative quantity of Hg accumulated in roots along the soil depths.

3.2. Characteristics of Hg Stable Isotopes in Soil and Roots. Figure 2a−f shows the Hg isotopic compositions in soils and roots along with the soil profiles. The δ^{202}Hg values in soils at three quadrats all displayed significantly increasing trends with ranges from −1.92‰ to −2.01‰ at the forest floor (0−15 cm) to −1.36‰ for LX at 410 cm, −1.07‰ for SN at 270 cm, and 0.72‰ for CW at 420 cm, respectively ($p < 0.01$ except $p = 0.24$ for the SN profile by two-tailed t test) (Table S1). The mean δ^{202}Hg value for unweathered rock was −0.12 ± 0.31‰ (Table S2). In contrast, the δ^{202}Hg values in roots are relatively constant (−2.04‰ to −2.76‰). The δ^{202}Hg values of fine roots were comparable for all three species, with values of −2.76 ± 0.31‰ for CW, −2.37 ± 0.35‰ for SN, and −2.47 ± 0.24‰ for LX ($p > 0.05$ by one-way ANOVA test, Table S4). Further comparison of Hg isotopic compositions in LX roots showed comparable δ^{202}Hg values between fine and medium roots (−2.47 ± 0.24‰ versus −2.35 ± 0.15‰, $p > 0.05$ by paired t test) but significantly more positive values for coarse roots (−2.04 ± 0.58‰) with a +0.40‰ shift compared to fine roots ($p < 0.05$ by paired t test). The mean δ^{202}Hg in the atmosphere was 0.24 ± 0.24‰,[6,49] in the mature foliage was −2.86 ± 0.27‰ to −3.40 ± 0.31‰,[6] in the stem was −2.36 ± 0.65‰, and in the bark was −2.34 ± 0.32‰ (Table S5).

https://doi.org/10.1021/acs.est.2c04217
Environ. Sci. Technol. 2022, 56, 14154−14165

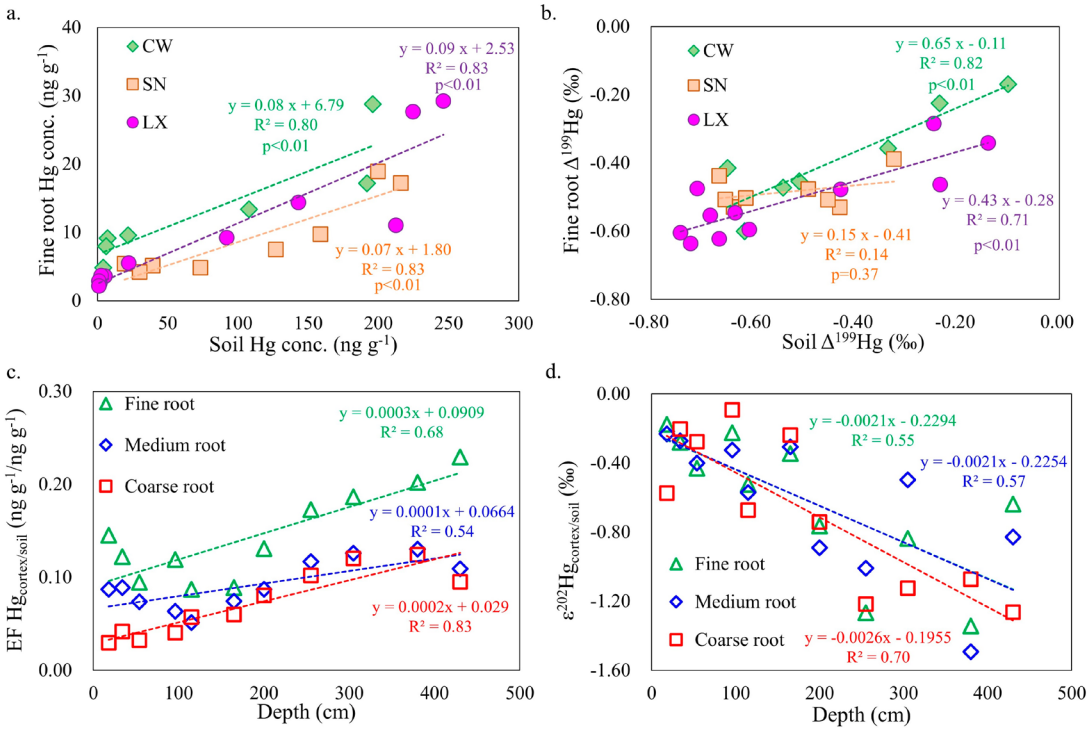

Figure 4. Correlation of (a) Hg concentration in fine roots versus soil, (b) Hg Δ^{199}Hg signature in fine roots versus soil, (c) LX root Hg concentration enrich factor versus soil depth, and (d) LX root δ^{202}Hg enrich factor between cortex and soil ($\varepsilon^{202}Hg_{cortex/soil}$) versus soil depth.

The Δ^{199}Hg values at three profiles showed slightly decreasing trends in the shallow 50−60 cm soils from −0.48‰ to −0.74‰ and significantly increasing trends from −0.12‰ to −0.20‰ at the bottom of the soil profiles. The Δ^{199}Hg values in LX fine, medium, and coarse roots showed similar trends (p > 0.05 by paired t test). The mean Δ^{199}Hg was −0.15 ± 0.07‰ in air,[6,49] from −0.28 ± 0.05‰ to −0.39 ± 0.06‰ in mature foliage,[6] −0.27 ± 0.10‰ in stem, and −0.45 ± 0.08‰ in bark, all significantly more positive than the signatures in shallow roots (p < 0.05 by independent t test). The three soil profiles and roots showed consistent Δ^{199}Hg/Δ^{201}Hg ratios at 1.16 ± 0.03‰ and 1.15 ± 0.03‰ by the Williamson−York bivariate regression method,[52] respectively (Figure S1). Finally, the Δ^{200}Hg values were −0.01 ± 0.04‰ for soil profiles and −0.01 ± 0.05‰ for all tree roots.

3.3. Variations of Hg Concentration and Isotopic Compositions in Root Components. Figure 3a shows the heterogeneous Hg concentration distribution in root tissues. The Hg concentration in the cortex is 2.4−3.5 times higher than that in stele (p < 0.05 by paired t test), suggesting Hg enrichment in the root cortex. Interestingly, the MDF and odd-MIF signatures in the cortex and stele were comparable among LX fine, medium, and coarse roots (Figure 3b and c, p > 0.05 by paired t test). The cortex and stele Hg MDF signatures were at −2.32 ± 0.20‰ versus −2.60 ± 0.36‰, −2.32 ± 0.20‰ versus −2.31 ± 0.50‰, and −2.38 ± 0.27‰ versus −2.57 ± 0.56‰ (p > 0.05 by paired t test) for fine, medium, and coarse roots, respectively. The cortex and stele Hg odd-MIF signatures were −0.50 ± 0.17‰ versus −0.49 ± 0.17‰, −0.49 ± 0.17‰ versus −0.49 ± 0.17‰, and −0.47 ± 0.17‰ versus −0.40 ± 0.19‰ (p > 0.05 by paired t test) for fine, medium, and coarse roots, respectively. The median values in cortex and stele showed differences for the samples of coarse roots, with values of −0.57‰ for the cortex versus −0.36‰ for stele (Figure 3c). Such a positive odd-MIF signal in stele is distinctive in greater than 50 cm depth root samples (Figure S2).

The fine whole root Hg concentrations and odd-MIF signatures display significant correlations to values in surrounding soil (R^2 > 0.70, p < 0.01 by two-tailed t test, except p = 0.37 for odd-MIF in fine root versus soil in SN, Figure 4a and b). Significant correlations also exist in the Hg concentrations and Δ^{199}Hg signatures between soils and coarse roots, except for a few SN coarse roots samples (Figure S3). In addition, the Hg concentration enrichment factors ($EF_{cortex/soil}$ = Conc. Hg_{cotrex}/Conc. Hg_{soil}) increased with soil depth, from 0.10 in shallow soil to 0.22 in bottom soil for fine roots (Figure 4c). For LX roots, the Hg enrichment factors of Hg MDF ($\varepsilon^{202}Hg_{cortex/soil}$ = $\delta^{202}Hg_{cortex}$ − $\delta^{202}Hg_{soil}$) decreased from −0.20‰ to −1.20 ‰ along with the soil profile (R^2 = 0.55−0.70, Figure 4d).

4. DISCUSSION

4.1. Discerning Hg Sources in Roots. Earlier studies have documented the pathways of foliage uptake of atmospheric Hg^0 and subsequent translocation into the aboveground woody biomass.[5,6,53] Foliage can take up atmospheric Hg^0 via stomata and nonstomata routes.[5,6,53] A portion of the incorporated Hg complexed with metallothionein then translocated from foliage to the aboveground woody biomass via phloem and xylem routes when accompanied with nutrient translocation in trees.[14,37,54] Given the absence of MIF during Hg translocation in vegetation, MIF signals are utilized for tracing Hg source apportionment in forest ecosystems.[14,37,55,56] One earlier study found that the Δ^{199}Hg and Δ^{200}Hg values of the shallow roots were comparable to signatures of foliage and surface soils, indicating that Hg in shallow roots is derived from atmospheric

https://doi.org/10.1021/acs.est.2c04217
Environ. Sci. Technol. 2022, 56, 14154−14165

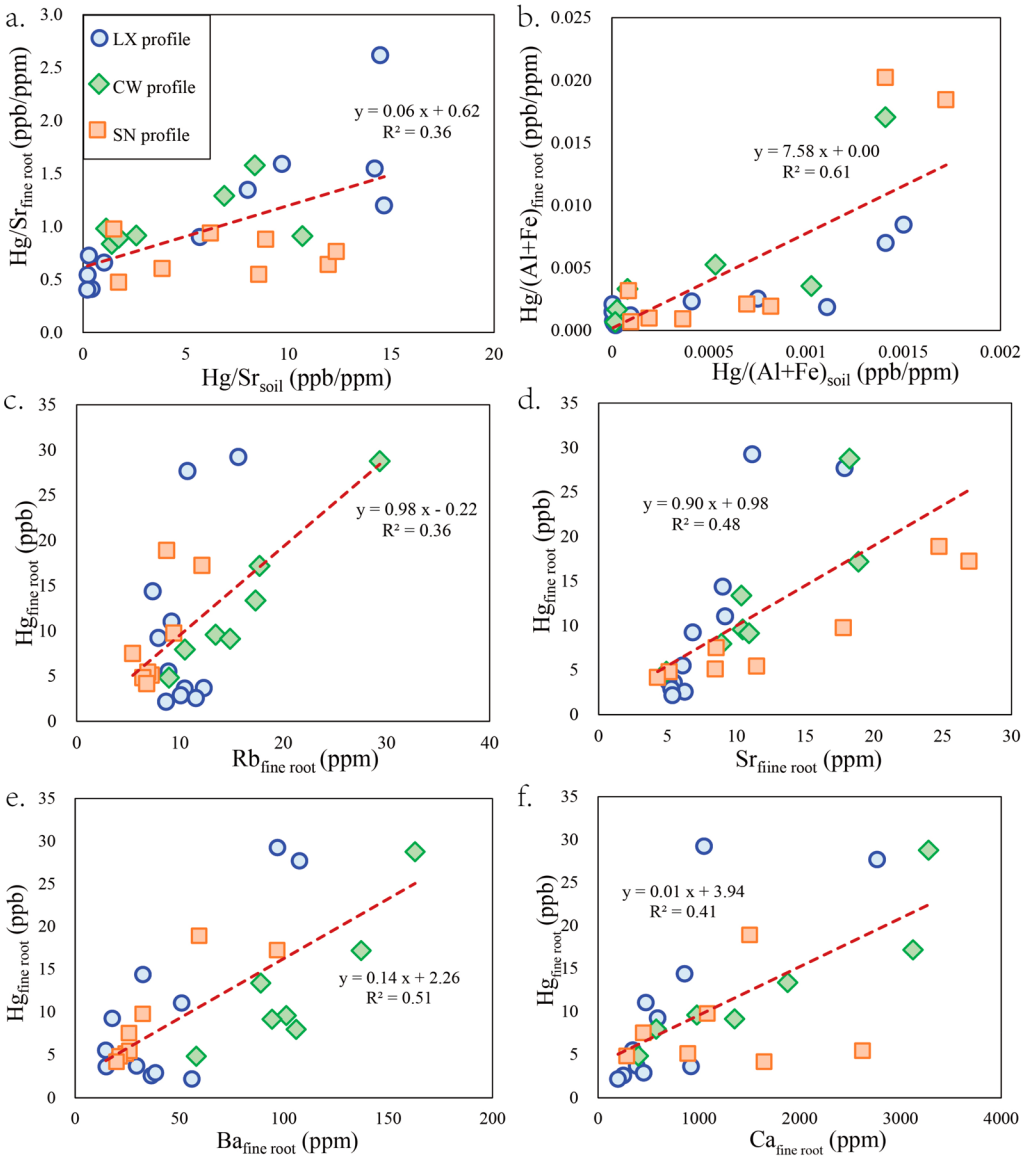

Figure 5. Correlation of geochemical variables in fine roots and soil profiles for (a) $Hg/Sr_{fine\ root}$ versus Hg/Sr_{soil} and (b) $Hg/(Al+Fe)_{fine\ root}$ versus $Hg/(Al+Fe)_{soil}$ and in fine roots for (c) Hg concentration versus Rb concentration, (d) Hg concentration versus Sr concentration, (e) Hg concentration versus Ba concentration, and (f) Hg concentration versus Ca concentration.

Hg^0 depositions,[14] but it could not distinguish whether the Hg direct translocation from foliage to root, or from litterfall Hg deposition into soils, is then uptaken by roots.

The comparable $\Delta^{199}Hg$ signatures (−0.30‰ to −0.50‰) among foliage Hg, stem Hg, and bark Hg (Figure 2d–f) confirm the earlier finding that vegetation uptake of atmospheric Hg^0 is the dominant Hg source for Hg accumulation in aboveground biomass. However, the −0.15‰ to −0.25‰ negative fractionation between shallow roots (−0.45‰ to −0.59‰) and foliage/stem suggests that the foliage Hg translocation is not the only source in the underground root. We offer observational evidence to show that Hg^{II} bound with lower molecular organic matter (such as cysteine) in a surrounding soil solution is likely the predominant source to enter into roots.[3,4,57,58] First, the Hg odd-MIF signatures along the soil profiles (Figure 2d –f) and strong correlations for Hg concentration and $\Delta^{199}Hg$ values between soils and fine roots (Figure 4a and b) support uptake of surrounding soil Hg as the predominant source in roots. In addition, significant positive correlations for the $\Delta^{199}Hg$ values between soils and cortexes ($R^2 > 0.90$) as well as steles (R^2 = 0.75–0.90) of LX roots further confirm that Hg translocations from the soils to cortexes and steles of roots occur (Figure S4). Moreover, the geochemical indicators also support this hypothesis due to the strongly positive correlations of Hg/Sr and Hg/(Al+Fe) ratios between soils and fine roots (Figure 5a and b). Given the element of Rb, Sr, Ba, and Ca in fine roots mainly from uptake of surrounding soils,[59,60] these elements showing significantly positive correlations to Hg in roots further suggest that root uptake of surrounding soil Hg dominate Hg sources in roots (Figure 5–f).

Our earlier studies explained Hg sources in soil profiles of ASSFERS.[28,39,61] Atmospheric Hg^0 deposition via litter input is the dominant source in surface soils. The slightly negative transition in odd-MIF signatures of shallow soils can be shaped by surface organosulfur photoreduction, and organic matter induced Hg dark reduction.[28] Geological Hg input caused by bedrock weathering with low Hg concentration and slight odd-

https://doi.org/10.1021/acs.est.2c04217
Environ. Sci. Technol. 2022, 56, 14154−14165

MIF signatures dominants Hg accumulation in deep soils.[28,61] It is noted that the elevated soil Hg concentration in the 165−200 cm depth SN profile does not cause enhanced Hg in roots, and this should be attributed to two possible causes. One is that the Hg concentration in roots is much lower than in soils; thus, the soil Hg increase would not lead to an obvious increase of root Hg due to the nonlinear response between soils and roots. Another is that geogenic Hg contributes the main sources of soil Hg speciation in deep soils, and the increase of such Hg concentration does not lead to a significant increase of bioavailable Hg concentration in deep soils. These negative Δ^{199}Hg values for the surface soils and roots (−0.44‰ to −0.68‰ for surface soils versus −0.45‰ to −0.59‰ for shallow roots) suggest that Hg stored in surface roots is derived from atmospheric Hg^0 deposition into soils and then uptake by roots. The positive odd-MIF signatures found in deep roots (e.g., root in C horizon soils with −0.34‰ to −0.20‰ of Δ^{199}Hg) are close to the signals of unweathered rock (−0.08‰ ± 0.06‰), indicating the geogenic Hg input into deep roots.

4.2. Processes of Root Uptake of Hg from Surrounding Soil. The larger specific surface area of fine roots contributes to greater Hg concentration, but the greater woody mass and longer lifespan of coarse roots can lead to a higher Hg mass (Figures 1a−c and 3a). The fine roots have a relatively short lifecycle and release most of the absorbed Hg to root rhizosphere soil due to the limited Hg transport to other parts of the tree. Given the reported fine root turnover (~0.83 yr^{-1}) for evergreen forest tree species,[62−64] we estimated 4.8−18.7 $\mu g\ m^{-2}\ yr^{-1}$ (mean: 12.2 ± 7.0 $\mu g\ m^{-2}\ yr^{-1}$) of fine root Hg returned back to soil, equivalent to 20%−78% of litterfall deposition at ASSFERS.[39] Such quick dynamic Hg exchange between fine roots and soils might accelerate Hg cycling in rhizosphere environments.

The soil pore Hg^0 gas diffusion driven by the gas gradient during the process of root respiration is one of the potential routes of root Hg uptake. The diffused Hg^0 gas could be quickly oxidized to Hg^{II} in root cells followed by liquid phase reactions. Similar processes also occur in the foliage.[6] Earlier studies at ASSFERS have depicted that microbial reduction induces no odd-MIF,[65,66] and abiotic dark reduction induced by nuclear volume effect[67] controls the quantity of pore Hg^0 gas in shallow soil,[28,41] resulting in an elevated Hg^0 gas concentration (4.0−15.9 ng m^{-3}) to promote gas diffusion. However, the total Hg gas volume and concentration in soil pores are still limited, especially in deep soil profiles (nearly close to 0 in the C horizon).[68−70] Therefore, soil pore Hg^0 gas may not be the sole source of Hg root uptake. In contrast, the diffusion of dissolved Hg^{II} driven by the Hg^{II} concentration gradient between soils and roots and the advection of water in roots are likely as main pathways for Hg uptake by roots.[71] Given the observed difference among ~0.00‰ of Δ^{200}Hg in roots, 0.25 ± 0.19‰ in precipitation,[5,31,32,72] and less than 10% contribution of the soil Hg source,[27,28] Hg^{II} wet deposition is not the main source of Hg^{II} in soil solutions. A more likely source is from desorption of soil Hg into the soil solution, which inherits the same isotopic signatures of soil Hg.[73]

To better understand the Hg uptake from surrounding soil by roots, we analyzed the gradients of Hg concentration and isotopic composition between the soil and the cortex of roots. The comparable odd-MIF signatures observed in soil and the cortex of fine roots ($p > 0.05$ paired t test) suggest negligible odd-MIF occurring during absorption−desorption processes in soils and Hg uptake by roots.[74] Interestingly, the enhancement factors (i.e., EF $Hg_{cortex/soil}$, Figure 4c) for fine, medium, and coarse root cortexes all increase with soil depth, but the negative transition of δ^{202}Hg (i.e., $\varepsilon^{202}Hg_{cortex/soil}$, Figure 4d) consistently decreases with the soil profiles ($R^2 = 0.55−0.70$, $p < 0.01$ by two-tailed t test). The relatively small enhancement factors at the surface soils might be caused by the shorter lifetime in surface roots than in deep soil roots,[75,76] which is beneficial to Hg detoxification for these tree species via part of root death.[12] The vertical decrease of $\varepsilon^{202}Hg_{cortex/soil}$ can be attributed to several causes. One is that Hg complexed with organic matter mainly occurs in surface soil that has high bioavailability, while a relatively inert Hg from the geogenic sources exists in deep soil.[77] The root Hg assimilation from deep soil is limited, which can induce a more significant fractionation of ^{202}Hg between the deep soil and cortex. In addition, Hg uptake by root cortexes is a dynamic process mediated by the vegetation biological processes (e.g., tree transpiration);[20] thus, the variation of root biological processes along with the soil profile is a supplemental explanation for such a MDF trend.

4.3. Processes of Hg Translocation in Roots. After the soil Hg uptake by the fine root cortex, Hg needs to traverse layers of plasma membrane, such as the endodermis,[59] into the root stele. The average of 2.5−3.5 times higher Hg concentration in the cortex than in stele ($p < 0.001$) suggests that only limited Hg can translocate into the root endodermis biomass. The EF ratios of Hg_{cortex}/Hg_{stele} are comparable for all roots. This is consistent with earlier studies reported values in other subtropical forests, such as 3.0−3.6 for *Ardisia quinquegona* and 2.2−4.0 for *Cinnamomum camphora*.[12] These data point to a small fraction of Hg uptake being translocated into root woody biomass with most Hg tightly bound to the cell walls and membranes of fine roots.[12]

The similar Hg isotopic compositions between the cortex and stele ($p > 0.05$ by paired t test, Figure 3b and c) suggest negligible isotopic fractionations during Hg translocation in roots. This indicates that the translocated Hg in roots is not in the form of Hg ions, possibly in complexed Hg to the reduced sulfur function groups (e.g., metalloprotein) that undergoes little fractionation.[78] The small differences of δ^{202}Hg values in all root samples and the decreasing Hg concentration from the fine to coarse roots (Figure 2a) indicate that the effect of Hg translocation from fine to coarse roots is much weaker than the effect of mass dilution caused by the growth of woody biomass. The positive odd-MIF and slightly negative MDF in stele than signatures in cortexes of coarse roots (Figure 3c and Figure S2) can be attributed to two reasons. One is by translocation of Hg with positive odd-MIF and negative values from aboveground tissues. We estimate a 20% contribution of Hg sources of surface roots from aboveground tissues by using a two-end member mass mixing model of odd-MIF (foliage Δ^{199}Hg versus soil Δ^{199}Hg) detailed in SI Section 2. Such an aboveground translocation into deep roots could have weakened along the soil depth. This is inconsistent with that more positive odd-MIF signatures in stele are found in the 50−150 cm depth soil rather than surface soil, and then, this might be not the sole reason. Another more possible cause is that the secondary reactions occurred at the rhizosphere soil, such as organic dark reduction[67] or absorption,[29] which induced an odd-MIF and MDF variation in the cortex and stele of coarse

https://doi.org/10.1021/acs.est.2c04217
Environ. Sci. Technol. 2022, 56, 14154−14165

roots. However, such processes are not well understood and require further investigation.

Transpiration induces a potential that moves water and dissolved inorganic elements from the roots to the aboveground biomass via the xylem route.[11] However, such water and nutrient transport leads to little Hg translocation, as indicated by the distinct Hg odd-MIF signatures along with root profiles to the aboveground stems, as well as similar Hg odd-MIF signatures between foliage and stems (Figure 1d–f). The limited Hg translocation may be explained by the small mobile Hg mass in the cell cytosolic of the xylem, which is too insignificant to be transported over a long distance in root woody biomass.[12]

5. IMPLICATIONS

In this study, we show the heterogeneities of Hg concentration and pool size distribution in roots of different diameters and in vertical soil profiles. Because of the highly uneven distribution, current estimates of Hg mass stored in underground biomasses have large uncertainties. If we apply the similar methodology of earlier studies with Hg concentration in fine roots and 0–50 cm depth roots, the estimated root Hg pool size is from 51 to 379 $\mu g\ m^{-2}$, causing 3–6 times higher overestimation (Table S6). Given the wide range of in-soil Hg concentration distribution,[3,79] the number of sample collection sites (~60) of global root Hg data sets obtained from scattered locations in China and Europe regions (Figure S2)[3,4,8] is insufficient to represent the variation of the global Hg spatial distribution. Moreover, root biomass largely depends on tree species and climate factors, and therefore, the heterogeneity of root mass across the globe is another constrain in quantifying Hg pool size in roots. More studies focus on the root Hg concentration across the globe, specifically in tropical forest with elevated root biomass[62,64] and greater than 45% of the global forest area.[38] The result from the typical subtropical forest provides an insight in understanding the trend of Hg accumulation in roots along with the soil depth. The findings were utilized to imply additional work needed to better understand the global Hg budget. Meanwhile, we recommend that additional measurements be made to better understand root Hg distribution at various depths and root size for a better estimation on root Hg storage.

The evidence from stable Hg isotopes supports that Hg in roots is predominantly derived from surrounding soil rather than atmospheric uptake of Hg^0 and that Hg acquired from root uptake is less mobile than foliage uptake of atmospheric Hg^0. These findings suggest that the Hg stored in roots originates from underground exchanges and does not contribute significantly to the source–sink terms of atmospheric Hg. We recommend more studies in obtaining data from forest ecosystems at global sites to further verify this hypothesis.

ASSOCIATED CONTENT

Supporting Information

The Supporting Information is available free of charge at https://pubs.acs.org/doi/10.1021/acs.est.2c04217.

Additional experimental details and data sets in Sections S1 and S2 and Tables S1–S6. Additional figures as mentioned in the text in Figures S1 and S2 (PDF)

AUTHOR INFORMATION

Corresponding Authors

Xun Wang – *State Key Laboratory of Environmental Geochemistry, Institute of Geochemistry, Chinese Academy of Sciences, Guiyang 550081, China;* orcid.org/0000-0002-7407-8965; Phone: +86-17785003956; Email: wangxun@mail.gyig.ac.cn

Xinbin Feng – *State Key Laboratory of Environmental Geochemistry, Institute of Geochemistry, Chinese Academy of Sciences, Guiyang 550081, China; Center for Excellence in Quaternary Science and Global Change, Chinese Academy of Sciences, Xi'an 710061, China;* orcid.org/0000-0002-7462-8998; Phone: +86-851-85895728; Email: fengxinbin@vip.skleg.cn

Authors

Wei Yuan – *State Key Laboratory of Environmental Geochemistry, Institute of Geochemistry, Chinese Academy of Sciences, Guiyang 550081, China*

Che-Jen Lin – *Center for Advances in Water and Air Quality, Lamar University, Beaumont, Texas 77710, United States*

Fei Wu – *State Key Laboratory of Environmental Geochemistry, Institute of Geochemistry, Chinese Academy of Sciences, Guiyang 550081, China; University of Chinese Academy of Sciences, Beijing 100049, China*

Kang Luo – *State Key Laboratory of Environmental Geochemistry, Institute of Geochemistry, Chinese Academy of Sciences, Guiyang 550081, China*

Hui Zhang – *State Key Laboratory of Environmental Geochemistry, Institute of Geochemistry, Chinese Academy of Sciences, Guiyang 550081, China*

Zhiyun Lu – *CAS Key Laboratory of Tropical Forest Ecology, Xishuangbanna Tropical Botanical Garden, Chinese Academy of Sciences, Mengla 666303, China*

Complete contact information is available at: https://pubs.acs.org/10.1021/acs.est.2c04217

Notes

The authors declare no competing financial interest.

ACKNOWLEDGMENTS

This work was funded by the National Natural Science Foundation of China (41829701 and 42007307) and China Postdoctoral Science Foundation (2020M673300). The data used in this study are tabulated in the SI.

REFERENCES

(1) Selin, H.; Keane, S. E.; Wang, S.; Selin, N. E.; Davis, K.; Bally, D. Linking science and policy to support the implementation of the Minamata Convention on Mercury. *Ambio* **2018**, *47* (2), 198–215.

(2) Outridge, P. M.; Mason, R. P.; Wang, F.; Guerrero, S.; Heimbürger-Boavida, L. E. Updated Global and Oceanic Mercury Budgets for the United Nations Global Mercury Assessment 2018. *Environ. Sci. Technol.* **2018**, *52* (20), 11466–11477.

(3) Wang, X.; Yuan, W.; Lin, C.-J.; Feng, X. Mercury cycling and isotopic fractionation in global forests. *Crit. Rev. Environ. Sci. Technol.* **2022**, *52*, 3763–3786.

(4) Zhou, J.; Obrist, D.; Dastoor, A.; Jiskra, M.; Ryjkov, A. Vegetation uptake of mercury and impacts on global cycling. *Nature Reviews Earth & Environment* **2021**, *2* (4), 269–284.

(5) Demers, J. D.; Blum, J. D.; Zak, D. R. Mercury isotopes in a forested ecosystem: Implications for air-surface exchange dynamics and the global mercury cycle. *Global Biogeochem Cy* **2013**, *27* (1), 222–238.

(6) Yuan, W.; Sommar, J.; Lin, C.-J.; Wang, X.; Li, K.; Liu, Y.; Zhang, H.; Lu, Z.; Wu, C.; Feng, X. Stable Isotope Evidence Shows Re-emission of Elemental Mercury Vapor Occurring after Reductive Loss from Foliage. *Environ. Sci. Technol.* **2019**, *53* (2), 651−660.
(7) Wang, X.; Bao, Z.; Lin, C.-J.; Yuan, W.; Feng, X. Assessment of Global Mercury Deposition through Litterfall. *Environ. Sci. Technol.* **2016**, *50* (16), 8548−8557.
(8) Zhou, J.; Obrist, D. Global Mercury Assimilation by Vegetation. *Environ. Sci. Technol.* **2021**, *55* (20), 14245−14257.
(9) Santoro, M.; Cartus, O.; Carvalhais, N.; Rozendaal, D. M. A.; Avitabile, V.; Araza, A.; de Bruin, S.; Herold, M.; Quegan, S.; Rodríguez-Veiga, P.; Balzter, H.; Carreiras, J.; Schepaschenko, D.; Korets, M.; Shimada, M.; Itoh, T.; Moreno Martínez, Á.; Cavlovic, J.; Cazzolla Gatti, R.; da Conceição Bispo, P.; Dewnath, N.; Labrière, N.; Liang, J.; Lindsell, J.; Mitchard, E. T. A.; Morel, A.; Pacheco Pascagaza, A. M.; Ryan, C. M.; Slik, F.; Vaglio Laurin, G.; Verbeeck, H.; Wijaya, A.; Willcock, S. The global forest above-ground biomass pool for 2010 estimated from high-resolution satellite observations. *Earth Syst. Sci. Data* **2021**, *13* (8), 3927−3950.
(10) Ma, H.; Mo, L.; Crowther, T. W.; Maynard, D. S.; van den Hoogen, J.; Stocker, B. D.; Terrer, C.; Zohner, C. M. The global distribution and environmental drivers of aboveground versus belowground plant biomass. *Nature Ecology & Evolution* **2021**, *5* (8), 1110−1122.
(11) Trakal, L.; Martínez-Fernández, D.; Vítková, M.; Komárek, M. Phytoextraction of Metals: Modeling Root Metal Uptake and Associated Processes. In *Phytoremediation: Management of Environmental Contaminants*, Vol. *1*; Ansari, A. A., Gill, S. S., Gill, R., Lanza, G. R.; Newman, L., Eds.; Springer International Publishing: Cham, 2015; pp 69−83.
(12) Wang, J.-J.; Guo, Y.-Y.; Guo, D.-L.; Yin, S.-L.; Kong, D.-L.; Liu, Y.-S.; Zeng, H. Fine Root Mercury Heterogeneity: Metabolism of Lower-Order Roots as an Effective Route for Mercury Removal. *Environ. Sci. Technol.* **2012**, *46* (2), 769−777.
(13) Cocking, D.; Rohrer, M.; Thomas, R.; Walker, J.; Ward, D. Effects of root morphology and Hg concentration in the soil on uptake by terrestrial vascular plants. *Water, Air, and Soil Pollution* **1995**, *80* (1), 1113−1116.
(14) Wang, X.; Yuan, W.; Lin, C.-J.; Luo, J.; Wang, F.; Feng, X.; Fu, X.; Liu, C. Underestimated Sink of Atmospheric Mercury in a Deglaciated Forest Chronosequence. *Environ. Sci. Technol.* **2020**, *54* (13), 8083−8093.
(15) Leonard, T. L.; Taylor, G. E., Jr.; Gustin, M. S.; Fernandez, G. C. J. Mercury and plants in contaminated soils: 1. Uptake, partitioning, and emission to the atmosphere. *Environ. Toxicol. Chem.* **1998**, *17* (10), 2063−2071.
(16) Cui, L.; Feng, X.; Lin, C. J.; Wang, X.; Meng, B.; Wang, X.; Wang, H. Accumulation and translocation of 198Hg in four crop species. *Environmental Toxicology & Chemistry* **2014**, *33* (2), 334−340.
(17) Pereira, E.; Vale, C.; Tavares, C. F.; Válega, M.; Duarte, A. C. Mercury in Plants from Fields Surrounding a Contaminated Channel of Ria de Aveiro, Portugal. *Soil and Sediment Contamination: An International Journal* **2005**, *14* (6), 571−577.
(18) Lindberg, S. E.; Jackson, D. R.; Huckabee, J. W.; Janzen, S. A.; Levin, M. J.; Lund, J. R. Atmospheric Emission and Plant Uptake of Mercury from Agricultural Soils near the Almaden Mercury Mine. *J. Environ. Qual* **1979**, *8* (4), 572−578.
(19) Luo, Y.; Duan, L.; Driscoll, C. T.; Xu, G. Y.; Shao, M. S.; Taylor, M.; Wang, S. X.; Hao, J. M. Foliage/atmosphere exchange of mercury in a subtropical coniferous forest in south China. *J. Geophys Res-Biogeo* **2016**, *121* (7), 2006−2016.
(20) Bishop, K. H.; Lee, Y.-H.; Munthe, J.; Dambrine, E. Xylem sap as a pathway for total mercury and methylmercury transport from soils to tree canopy in the boreal forest. *Biogeochemistry* **1998**, *40* (2), 101−113.
(21) Mao, Y.; Li, Y.; Richards, J.; Cai, Y. Investigating Uptake and Translocation of Mercury Species by Sawgrass (Cladium jamaicense) Using a Stable Isotope Tracer Technique. *Environ. Sci. Technol.* **2013**, *47* (17), 9678−9684.
(22) Meng, B.; Li, Y.; Cui, W.; Jiang, P.; Liu, G.; Wang, Y.; Richards, J.; Feng, X.; Cai, Y. Tracing the Uptake, Transport, and Fate of Mercury in Sawgrass (Cladium jamaicense) in the Florida Everglades Using a Multi-isotope Technique. *Environ. Sci. Technol.* **2018**, *52* (6), 3384−3391.
(23) Yin, R.; Feng, X.; Meng, B. Stable Mercury Isotope Variation in Rice Plants (Oryza sativa L.) from the Wanshan Mercury Mining District, SW China. *Environ. Sci. Technol.* **2013**, *47* (5), 2238−2245.
(24) Huang, S.; Jiang, R.; Song, Q.; Zhang, Y.; Huang, Q.; Su, B.; Chen, Y.; Huo, Y.; Lin, H. Study of mercury transport and transformation in mangrove forests using stable mercury isotopes. *Sci. Total Environ.* **2020**, *704*, 135928.
(25) Yu, B.; Fu, X. W.; Yin, R. S.; Zhang, H.; Wang, X.; Lin, C. J.; Wu, C. S.; Zhang, Y. P.; He, N. N.; Fu, P. Q.; Wang, Z. F.; Shang, L. H.; Sommar, J.; Sonke, J. E.; Maurice, L.; Guinot, B.; Feng, X. B. Isotopic Composition of Atmospheric Mercury in China: New Evidence for Sources and Transformation Processes in Air and in Vegetation. *Environ. Sci. Technol.* **2016**, *50* (17), 9262−9269.
(26) Xia, S.; Yuan, W.; Lin, L.; Yang, X.; Feng, X.; Li, X.; Liu, X.; Chen, P.; Zeng, S.; Wang, D.; Su, Q.; Wang, X. Latitudinal gradient for mercury accumulation and isotopic evidence for post-depositional processes among three tropical forests in Southwest China. *J. Hazard Mater.* **2022**, *429*, 128295.
(27) Jiskra, M.; Wiederhold, J. G.; Skyllberg, U.; Kronberg, R.-M.; Hajdas, I.; Kretzschmar, R. Mercury Deposition and Re-emission Pathways in Boreal Forest Soils Investigated with Hg Isotope Signatures. *Environ. Sci. Technol.* **2015**, *49* (12), 7188−7196.
(28) Yuan, W.; Wang, X.; Lin, C.-J.; Wu, C.; Zhang, L.; Wang, B.; Sommar, J.; Lu, Z.; Feng, X. Stable Mercury Isotope Transition during Postdepositional Decomposition of Biomass in a Forest Ecosystem over Five Centuries. *Environ. Sci. Technol.* **2020**, *54* (14), 8739−8749.
(29) Guedron, S.; Arnouroux, D.; Tessier, E.; Grirnaldi, C.; Barre, J.; Berail, S.; Perrot, V.; Grimaldi, M. Mercury Isotopic Fractionation during Pedogenesis in a Tropical Forest Soil Catena (French Guiana): Deciphering the Impact of Historical Gold Mining. *Environ. Sci. Technol.* **2018**, *52* (20), 11573−11582.
(30) Chen, J.; Hintelmann, H.; Feng, X.; Dimock, B. Unusual fractionation of both odd and even mercury isotopes in precipitation from Peterborough, ON, Canada. *Geochim Cosmochim Ac* **2012**, *90*, 33−46.
(31) Li, K.; Lin, C.-J.; Yuan, W.; Sun, G.; Fu, X.; Feng, X. An improved method for recovering and preconcentrating mercury in natural water samples for stable isotope analysis. *J. Anal Atom Spectrom* **2019**, *34* (11), 2303−2313.
(32) Gratz, L. E.; Keeler, G. J.; Blum, J. D.; Sherman, L. S. Isotopic Composition and Fractionation of Mercury in Great Lakes Precipitation and Ambient Air. *Environ. Sci. Technol.* **2010**, *44* (20), 7764−7770.
(33) Blum, J. D.; Sherman, L. S.; Johnson, M. W. Mercury Isotopes in Earth and Environmental Sciences. *Annu. Rev. Earth Pl Sc* **2014**, *42*, 249−269.
(34) Smith, C. N.; Kesler, S. E.; Blum, J. D.; Rytuba, J. J. Isotope geochemistry of mercury in source rocks, mineral deposits and spring deposits of the California Coast Ranges, USA. *Earth Planet Sc Lett.* **2008**, *269* (3), 399−407.
(35) Wang, X.; Luo, J.; Yuan, W.; Lin, C.-J.; Wang, F.; Liu, C.; Wang, G.; Feng, X. Global warming accelerates uptake of atmospheric mercury in regions experiencing glacier retreat. *Proc. Natl. Acad. Sci. U. S. A.* **2020**, *117* (4), 2049−2055.
(36) Obrist, D.; Agnan, Y.; Jiskra, M.; Olson, C. L.; Colegrove, D. P.; Hueber, J.; Moore, C. W.; Sonke, J. E.; Helmig, D. Tundra uptake of atmospheric elemental mercury drives Arctic mercury pollution. *Nature* **2017**, *547* (7662), 201−204.
(37) Wang, X.; Yuan, W.; Lin, C.-J.; Wu, F.; Feng, X. Stable mercury isotopes stored in Masson Pinus tree rings as atmospheric mercury archives. *J. Hazard Mater.* **2021**, *415*, 125678.
(38) *The State of the World's Forests 2020*, FAO, 2021.

(39) Yuan, W.; Wang, X.; Lin, C.-J.; Zhang, H.; Feng, X.; Lu, Z. Impacts of Extreme Weather on Mercury Uptake and Storage in Subtropical Forest Ecosystems. *J. Geophys Res-Biogeo* **2022**, *127* (1), No. e2021JG006681.
(40) Lu, Z.; Yuan, W.; Luo, K.; Wang, X. Litterfall mercury reduction on a subtropical evergreen broadleaf forest floor revealed by multi-element isotopes. *Environ. Pollut.* **2021**, *268*, 115867.
(41) Yuan, W.; Wang, X.; Lin, C.-J.; Sommar, J. O.; Wang, B.; Lu, Z.; Feng, X. Quantification of Atmospheric Mercury Deposition to and Legacy Re-emission from a Subtropical Forest Floor by Mercury Isotopes. *Environ. Sci. Technol.* **2021**, *55* (18), 12352−12361.
(42) Tan, Z. H.; Zhang, Y. P.; Schaefer, D.; Yu, G. R.; Liang, N.; Song, Q. H. An old-growth subtropical Asian evergreen forest as a large carbon sink. *Atmos. Environ.* **2011**, *45* (8), 1548−1554.
(43) Wang, B.; Yuan, W.; Wang, X.; Li, K.; Lin, C.-J.; Li, P.; Lu, Z.; Feng, X.; Sommar, J. Canopy-Level Flux and Vertical Gradients of Hg0 Stable Isotopes in Remote Evergreen Broadleaf Forest Show Year-Around Net Hg0 Deposition. *Environ. Sci. Technol.* **2022**, *56* (9), 5950−5959.
(44) Yang, Z.; Yang, X. D. Characteristics of floor litter and soil arthropod community in different types ot subtropical forest in Ailao Mountain of Yunnan, Southwest China. *Ying Yong Sheng Tai Xue Bao* **2011**, *22* (11), 3011−3020.
(45) Wang, X.; Yuan, W.; Feng, X.; Wang, D.; Luo, J. Moss facilitating mercury, lead and cadmium enhanced accumulation in organic soils over glacial erratic at Mt. Gongga, China. *Environ. Pollut.* **2019**, *254*, 112974.
(46) Sun, R. Y.; Enrico, M.; Heimburger, L. E.; Scott, C.; Sonke, J. E. A double-stage tube furnace-acid-trapping protocol for the pre-concentration of mercury from solid samples for isotopic analysis. *Anal Bioanal Chem.* **2013**, *405* (21), 6771−6781.
(47) Fu, X.; Heimbuerger, L.-E.; Sonke, J. E. Collection of atmospheric gaseous mercury for stable isotope analysis using iodine- and chlorine-impregnated activated carbon traps. *J. Anal Atom Spectrom* **2014**, *29* (5), 841−852.
(48) *U.S. EPA Method 1631. Revision E: Mercury in Water by Oxidation, Purge and Trap, and Cold Vapor Atomic Fluorescence Spectrometry*; U.S. EPA, 2002.
(49) Fu, X.; Zhang, H.; Liu, C.; Zhang, H.; Lin, C.-J.; Feng, X. Significant Seasonal Variations in Isotopic Composition of Atmospheric Total Gaseous Mercury at Forest Sites in China Caused by Vegetation and Mercury Sources. *Environ. Sci. Technol.* **2019**, *53* (23), 13748−13756.
(50) Bergquist, B. A.; Blum, J. D. Mass-dependent and -independent fractionation of Hg isotopes by photoreduction in aquatic systems. *Science* **2007**, *318* (5849), 417−420.
(51) Estrade, N.; Carignan, J.; Sonke, J. E.; Donard, O. F. X. Measuring Hg Isotopes in Bio-Geo-Environmental Reference Materials. *Geostand Geoanal Res.* **2010**, *34* (1), 79−93.
(52) Cantrell, C. A. Technical Note: Review of methods for linear least-squares fitting of data and application to atmospheric chemistry problems. *Atmos Chem. Phys.* **2008**, *8* (17), 5477−5487.
(53) Zheng, W.; Obrist, D.; Weis, D.; Bergquist, B. A. Mercury isotope compositions across North American forests. *Global Biogeochem Cy* **2016**, *30* (10), 1475−1492.
(54) Sun, L. M.; Lu, B. Y.; Yuan, D. X.; Hao, W. B.; Zheng, Y. Variations in the isotopic composition of stable mercury isotopes in typical mangrove plants of the Jiulong estuary, SE China. *Environmental Science and Pollution Research* **2017**, *24* (2), 1459−1468.
(55) Olson, C. L.; Jiskra, M.; Sonke, J. E.; Obrist, D. Mercury in tundra vegetation of Alaska: Spatial and temporal dynamics and stable isotope patterns. *Sci. Total Environ.* **2019**, *660*, 1502−1512.
(56) Wang, X.; Luo, J.; Yin, R.; Yuan, W.; Lin, C.-J.; Sommar, J.; Feng, X.; Wang, H.; Lin, C. Using Mercury Isotopes To Understand Mercury Accumulation in the Montane Forest Floor of the Eastern Tibetan Plateau. *Environ. Sci. Technol.* **2017**, *51* (2), 801−809.
(57) Feng, R.; Wei, C.; Tu, S. The roles of selenium in protecting plants against abiotic stresses. *Environmental and Experimental Botany* **2013**, *87*, 58−68.
(58) Wang, X.; Tam, N. F.-Y.; Fu, S.; Ametkhan, A.; Ouyang, Y.; Ye, Z. Selenium addition alters mercury uptake, bioavailability in the rhizosphere and root anatomy of rice (Oryza sativa). *Annals of Botany* **2014**, *114* (2), 271−278.
(59) Wang, H.; Inukai, Y.; Yamauchi, A. Root Development and Nutrient Uptake. *Critical Reviews in Plant Sciences* **2006**, *25* (3), 279−301.
(60) Shahid, M.; Dumat, C.; Khalid, S.; Schreck, E.; Xiong, T.; Niazi, N. K. Foliar heavy metal uptake, toxicity and detoxification in plants: A comparison of foliar and root metal uptake. *J. Hazard Mater.* **2017**, *325*, 36−58.
(61) Wang, X.; Yuan, W.; Lu, Z.; Lin, C.-J.; Yin, R.; Li, F.; Feng, X. Effects of Precipitation on Mercury Accumulation on Subtropical Montane Forest Floor: Implications on Climate Forcing. *Journal of Geophysical Research: Biogeosciences* **2019**, *124* (4), 959−972.
(62) Jackson, R. B.; Mooney, H. A.; Schulze, E. D. A global budget for fine root biomass, surface area, and nutrient contents. *Proc. Natl. Acad. Sci. U. S. A* **1997**, *94* (14), 7362−7366.
(63) Gill, R. A.; Jackson, R. B. *Global Distribution of Root Turnover in Terrestrial Ecosystems*; ORNL Distributed Active Archive Center, 2003.
(64) GILL, R. A.; JACKSON, R. B. Global patterns of root turnover for terrestrial ecosystems. *New Phytol* **2000**, *147* (1), 13−31.
(65) Kritee, K.; Blum, J. D.; Barkay, T. Mercury Stable Isotope Fractionation during Reduction of Hg(II) by Different Microbial Pathways. *Environ. Sci. Technol.* **2008**, *42* (24), 9171−9177.
(66) Kritee, K.; Blum, J. D.; Johnson, M. W.; Bergquist, B. A.; Barkay, T. Mercury stable isotope fractionation during reduction of Hg(II) to Hg(0) by mercury resistant microorganisms. *Environ. Sci. Technol.* **2007**, *41* (6), 1889−1895.
(67) Zheng, W.; Hintelmann, H. Nuclear Field Shift Effect in Isotope Fractionation of Mercury during Abiotic Reduction in the Absence of Light. *J. Phys. Chem. A* **2010**, *114* (12), 4238−4245.
(68) Obrist, D.; Pokharel, A. K.; Moore, C. Vertical Profile Measurements of Soil Air Suggest Immobilization of Gaseous Elemental Mercury in Mineral Soil. *Environ. Sci. Technol.* **2014**, *48* (4), 2242−2252.
(69) Moore, C. W.; Castro, M. S. Investigation of factors affecting gaseous mercury concentrations in soils. *Sci. Total Environ.* **2012**, *419*, 136−143.
(70) Sigler, J. M.; Lee, X. Gaseous mercury in background forest soil in the northeastern United States. *J. Geophys. Res.-Biogeo.* **2006**, *111*, G2.
(71) Jungk, A. Dynamics of Nutrient Movement at the Soil-Root Interface. In *Dynamics of Nutrient Movement at the Soil-Root Interface*; Waisel, Y., Eshel, A., Kafkafi, U., Eds.; Marcel Dekker, Inc., 2002.
(72) Chen, J. B.; Hintelmann, H.; Feng, X. B.; Dimock, B. Unusual fractionation of both odd and even mercury isotopes in precipitation from Peterborough, ON, Canada. *Geochim. Cosmochim. Acta* **2012**, *90*, 33−46.
(73) Woerndle, G. E.; Tsz-Ki Tsui, M.; Sebestyen, S. D.; Blum, J. D.; Nie, X. P.; Kolka, R. K. New Insights on Ecosystem Mercury Cycling Revealed by Stable Isotopes of Mercury in Water Flowing from a Headwater Peatland Catchment. *Environ. Sci. Technol.* **2018**, *52* (4), 1854−1861.
(74) Jiskra, M.; Wiederhold, J. G.; Bourdon, B.; Kretzschmar, R. Solution Speciation Controls Mercury Isotope Fractionation of Hg(II) Sorption to Goethite. *Environ. Sci. Technol.* **2012**, *46* (12), 6654−6662.
(75) Houde, S.; Thivierge, M. N.; Fort, F.; Bélanger, G.; Chantigny, M. H.; Angers, D. A.; Vanasse, A. J. P. Root growth and turnover in perennial forages as affected by management systems and soil depth. *Plant Soil* **2020**, *451*, 371−387.
(76) Rasse, D. P.; Rumpel, C.; Dignac, M.-F. Is soil carbon mostly root carbon? Mechanisms for a specific stabilisation. *Plant and Soil* **2005**, *269* (1), 341−356.
(77) Yin, R.; Feng, X.; Wang, J.; Bao, Z.; Yu, B.; Chen, J. Mercury isotope variations between bioavailable mercury fractions and total

mercury in mercury contaminated soil in Wanshan Mercury Mine, SW China. *Chem. Geol.* **2013**, *336*, 80−86.
(78) Jiskra, M.; Wiederhold, J. G.; Skyllberg, U.; Kronberg, R. M.; Kretzschmar, R. Source tracing of natural organic matter bound mercury in boreal forest runoff with mercury stable isotopes. *Environmental Science Processes & Impacts* **2017**, *19* (10), 1235.
(79) Wang, X.; Yuan, W.; Lin, C.-J.; Zhang, L.; Zhang, H.; Feng, X. Climate and Vegetation As Primary Drivers for Global Mercury Storage in Surface Soil. *Environ. Sci. Technol.* **2019**, *53* (18), 10665−10675.

https://doi.org/10.1021/acs.est.2c04217
Environ. Sci. Technol. 2022, 56, 14154−14165